SSRG International Journal of Electrical and Electronics Engineering
ISSN: 2348-8379/ https://doi.org/10.14445/23488379/IJEEE-V12I9P121

Volume 12 Issue 9, 202-214, September 2025

Original Article

Multi-Objective Whole Slide Image Segmentation Using Nature Inspired Whale Optimization Algorithm

K P Shivamurthy[1,2], Raju A S[3]

[1] *Research Scholar, SSAHE, Tumakuru, Karnataka, India*
[2]*Department of Electrical and Electronics Engineering, Cambridge Institute of Technology, Bengaluru, Karnataka, India*
[3] *Professor & Head, Department of Medical Electronics Engineering, SSIT, Tumakuru, India*

[1]*Corresponding Author : shivayash@gmail.com*

Received: 16 July 2025 Revised: 17 August 2025 Accepted: 16 September 2025 Published: 30 September 2025

Abstract - *For precise histopathological image analysis and classification, segmentation is a critical step that must be carried out accurately. Segmentation aids early detection and diagnosis of tumor and cancerous cells. Machine learning and artificial intelligence processes play a vital role in image processing applications. In this proposed work, the nature-inspired Whale Optimization Algorithm is used for the segmentation of whole slide images through multi-objective image thresholding. The images are subjected to initial pre-processing to eliminate disturbance and enhancement, followed by the application of the best threshold value. Various histopathology images are examined to validate the efficiency and versatility of the proposed methodology. A Dice coefficient of 50.8, a Jaccard index of 51.33, a Precision of 51.22, a Sensitivity of 71.59, an Accuracy of 91.86, an F-measure of 50.76, and a Specificity of 71.17 were the average results obtained for the tested images using the proposed system. The outcomes are assessed with other common segmentation approaches, validating the algorithm.*

Keywords - *Histopathology image, Image segmentation, Multi-objective optimization, Otsu thresholding, Whale optimization algorithm.*

1. Introduction

Automated image analysis is now possible for Whole-Slide Images (WSIs) due to their digitization in pathology. Pathological analysis is a long, difficult, and knowledge-exhaustive process. Over the last ten years, a major change has been seen in the pathological field due to the swift growth of artificial intelligence. The benefits of digital pathology include ease of storage, remote diagnosis capabilities, and the utilization of image analysis, hence improving the precision and accuracy of the diagnostic procedure. A fully automated method of assessment is anticipated in the future because of advancements in artificial intelligence, thus helping pathologists. The effective application of artificial intelligence algorithms to WSIs may result in the development of new clinical instruments that are more objective, repeatable, and accurate than those employed presently in routine clinical settings [1]. Subsamples of pictures or tiles are employed for WSI analysis because of the vast size of WSIs. Studies show that only 22% of the WSI's total area is made up of relevant tissue [2]. To avoid analyzing the entire WSI needlessly, the tissue segment has to be highlighted. Therefore, correctly identifying and separating these tissue patches from the background is an essential initial step before classifying tumor cells from healthy cells [3, 4]. Thresholding is a popular, practical, and computationally efficient segmentation technique for identifying Regions Of Interest (ROI) in high-resolution histopathology images. It works by dividing pixels into background and foreground according to their intensity values, frequently with the use of the image's histogram [5], [6]. Otsu's method, which optimizes the variation among classes, is one of the most often used automatic thresholding techniques [7]. The challenging issue of determining the optimal threshold values can be tackled as a single-objective or multi-objective optimization. Nature-inspired metaheuristic optimization techniques have been widely used recently to solve this issue [8, 9]. Additionally, several studies have presented ROI segmentation for histopathology images using swarm intelligence algorithms. These methods often maximize a single objective function, such as Kapur's entropy or Otsu's variance. Though multi-objective optimization is known for its benefits, such as maintaining population variety, improving convergence to genuine Pareto-optimal front and offering a solution reflecting trade-off between several objectives [10], its application for segmentation of whole slide images remains unexplored. While single-objective methods are useful for maximizing a particular metric, they frequently fall short of the intricate practical needs of histopathology segmentation, where it is critical for diagnostic reliability to balance the drop in false positives and false negatives. An exclusive Multi-Objective Whale Optimization Algorithm

(MOWOA) to accomplish optimal thresholding-based WSI segmentation is proposed in this work, directly addressing this gap. Because of its strong convergence rate, capacity to break out of local optima, and proven effectiveness in engineering applications, the Whale Optimization Algorithm (WOA) is selected in this work [11-13]. Developing a segmentation framework that concurrently maximizes three important goals: maximizing between-class variation, minimizing false positives, and decreasing false negatives, is the key objective of the proposed work. Unlike single-objective approaches, this methodology guarantees a balanced and robust segmentation performance. The key contributions are:

- To attain a clinically significant balance between various error types, a unique Multi-Objective WOA (MOWOA) model is proposed for histopathology image thresholding, incorporating three distinct segmentation objectives.
- The algorithm's versatility and generalizability are demonstrated by thorough validation on a wide range of WSIs.
- The competence of the MOWOA technique for effective segmentation is validated through various performance metrics.
- The proposed model's performance is compared to other popular approaches, including Otsu with PSO and single-objective WOA versions, to verify its superiority.

This paper's remaining sections are organised as follows. Section 2 presents the literature review, and Section 3 portrays the methodologies and workflow of the proposed study. Next, Section 4 gives the details of the dataset considered for the study, while Section 5 gives the results obtained. Further, Section 6 illustrates the discussion and inferences drawn, and the paper is concluded in the final section.

2. Related Works

Whole Slide Image (WSI) segmentation is a cornerstone of digital pathology, enabling the analysis of high-resolution histopathological images for disease diagnosis, prognosis, and research. WSIs are characterized by their massive size, complex tissue structures, and variability in staining protocols, making segmentation a challenging yet essential task. Over time, numerous approaches have been developed to address these problems, ranging from complex deep learning models to traditional image processing techniques. Below is a detailed thematic review of WSI segmentation, supported by an extensive literature review.

2.1. Tissue Region Segmentation

Tissue region segmentation aims to separate different tissue types, such as tumor, stroma, and necrosis, within WSIs. Early methods relied on thresholding and morphological operations for coarse segmentation [14]. Handcrafted elements like texture and color were used to increase accuracy through machine learning approaches like Random Forest and Support Vector Machines [15]. However, this field has undergone a revolution with the emergence of deep learning algorithms. U-Net, a Convolutional Neural Network (CNN) architecture, is one of the best-performing methodologies because of its capacity to process minimal datasets and generate accurate results [16]. Extensions like ResUNet and Attention U-Net have further enhanced performance by incorporating residual connections and attention mechanisms [17]. Recent advancements include vision transformers, which have shown promise in capturing long-range dependencies in WSIs [18]. Despite these advancements, challenges such as staining variability and tissue heterogeneity persist, necessitating robust pre-processing and normalization techniques.

2.2. Lesion and Tumor Segmentation

Accurate segmentation of lesions and tumors is essential for cancer diagnosis and treatment planning. Traditional methods like active contour models and region-growing algorithms have been used for lesion detection [19]. Machine learning techniques, such as feature-based classifiers, improved tumor segmentation by incorporating texture and shape features [20]. In tumor segmentation, fully convolutional networks and attention-based architectures have attained cutting-edge results [21]. TransUNet, for example, enables accurate tumor border delineation by combining transformers and CNNs to identify a local and global framework [22]. Recent advancements include Swin-UNet, which leverages shifted window transformers for improved tumor segmentation [18]. Challenges such as heterogeneous tumor morphology and class imbalance continue to drive research in this area.

2.3. Gland Segmentation

Gland segmentation is particularly important in colorectal and prostate cancer analysis. Traditional methods, such as morphological operations and edge detection, have been used for gland boundary identification [23]. Machine learning approaches, including graph-based methods, improved gland segmentation by modelling spatial relationships between glandular structures [24]. Deep learning models, such as Gland-Net and Micro-Net, have been specifically designed for gland segmentation, achieving high accuracy in complex datasets [25, 26]. Recent works, such as Gland Vision, have introduced transformer-based architectures for gland segmentation, achieving superior performance in challenging datasets [27]. Challenges like glandular variability and lumen detection remain active areas of research.

2.4. Supervised and Unsupervised Segmentation

The reliance on large, annotated datasets is a significant bottleneck in WSI segmentation. Models with slide-level labels have been trained using weakly supervised learning techniques like Multiple Instance Learning (MIL), eliminating the necessity of pixel-level annotations [28]. Unsupervised

learning techniques, such as clustering and self-supervised learning, have also been explored for WSI segmentation [25]. Recent works like WSI-MIL have introduced transformer-based MIL frameworks for improved weakly supervised segmentation [29]. These approaches are particularly useful in low-resource settings where annotated data is scarce.

2.5. Evolutionary Algorithms for Segmentation

Using nature-inspired optimisation algorithms to obtain the best threshold as an optimization problem is a prevailing method that has been extensively employed by the authors in the recent past. To name a few, manta ray foraging optimization algorithm [30], enhanced equilibrium optimizer [31], hybrid marine predator algorithm with salp swarm algorithm [32], opposition-based Lévy Flight chimp optimizer [33], black widow optimization algorithm [34] and cuckoo search algorithm [35].

These techniques were used on various benchmark images, COVID-19 CT images, and thermography pictures. [36] suggests using an improved particle swarm optimization to perform multi-threshold segmentation of an image based on Otsu's method. Authors in [37] provide information on the choice of the threshold value and summarise the usage of Otsu's method in image segmentation. [38] proposed adaptive thresholding method that uses the mean and standard deviation to threshold images, enhancing the image segmentation quality.

The Otsu method with fuzzy logic was applied to obtain the best threshold for various types of pictures in [39]. Particle swarm optimization was combined with Otsu thresholding for lung CT image segmentation in [40]. The opposition-based Manta Ray foraging optimization was used to identify regions of interest in CT images of COVID patients in [41]. Multi-level thresholding was carried out for COVID CT images utilizing the equilibrium optimizer algorithm in [31]. Various studies used swarm-based optimization methods to find the best threshold for various types of benchmark images and medical images. A hybrid methodology for cytology image segmentation was employed in [42] using gray wolf optimization and fuzzy clustering. Wavelet method and WOA were combined for CT and MR image segmentation in [43]. The authors in [32] employed a Gaussian barebone salp swarm algorithm in combination with a stochastic fractal search technique to segment CT COVID-19 images. In [44], the Firefly algorithm was used to find the optimum threshold for the segmentation of breast cancer images. A grouping model for breast histopathology images was published by the authors in [45], utilizing the Cuckoo search algorithm. In addition, a summary of various optimization approaches for image segmentation is provided in Table 1. It is observed from the literature review that there have not been many studies on using multi-objective problems to segment whole slide images. As a result, this paper presents a multi-objective whale optimization technique that determines the ideal threshold for the entire slide picture segmentation.

Table 1. List of works adopting optimization techniques for image segmentation

Reference	Algorithm	Type of Image	Objective
[31]	Moth Flame Optimization and Whale optimization algorithm	Benchmark images	Otsu’s objective function was used for segmentation
[32]	Artificial bee colony and Sine-cosine algorithm	Images from art explosion database	Multilevel thresholding for image segmentation was implemented. To improve performance, the ABC used SCA as a local search.
[33]	Harris Hawks Optimization	Mammography images	When segmenting images, minimal cross-entropy was used as a fitness function. Two machine learning algorithms and other similar optimizers are used for validation.
[34]	Firefly Optimization	Standard images	Multilevel segmentation for maximizing Otsu’s variance was employed in this work.
[14]	Equilibrium optimizer	Test images from Berkley University	An objective function based on Kapur entropy was utilized and compared with seven other algorithms for performance evaluation.
[35]	Cuckoo Search Algorithm	Satellite images	Otsu and Kapur's method is used to address the color image segmentation problem.
[36]	Artificial Bee Colony	Standard Images	Otsu thresholding using the ABC algorithm for image segmentation was proposed in this work.
[37]	Particle swarm optimization	Standard Images	This method was employed to split the color images based on pixels.
[38]	Whale optimization algorithm, grey wolf optimizer and PSO	Benchmark Test Images	Multilevel thresholding for image segmentation was carried out on twenty benchmark test images to maximize the Otsu approach.

[16]	Firefly algorithm	Satellite images and Standard Text Images	A multilevel thresholding technique with a fitness function as fuzzy entropy for color images was carried out.
[39]	Particle swarm optimization	Benchmark images	This study used Kapur's entropy as the objective function to create a non-revisiting quantum-inspired PSO method aimed at finding the best multilevel thresholds for grayscale images.
[40]	Teaching a learning-based optimization algorithm	Standard test images	Otsu and Kapur's entropy objective functions were applied to 10 typical test images using the TLBO algorithm.
[41]	Differential Evolution method	Real-life true color images and satellite images.	A beta differential evolution-based multilevel thresholding for color images with two distinct objective functions is proposed.
[17]	Black Widow optimization algorithm	Benchmark images	The algorithm employed two different fitness functions - the Otsu and Kapur algorithms- to obtain an optimal threshold value and evaluate the multilevel image segmentation problem.
[30]	Elephant herding optimization	Standard test images	Outcome-based learning and dynamic Cauchy mutation, maximizing the difference between classes and Kapur's entropy for multilevel image thresholding.

3. Proposed Work and Methodologies

Here, the workflow and the methodologies used are presented in detail. The basic whale optimization algorithm and fundamental Otsu thresholding are explained, which are the foundation for developing the proposed methodology. Figure 1 demonstrates the workflow of the proposed algorithm. Once the images are read, they are transformed into grayscale images. In the next step, photos are tiled with 128x128 pixel dimensions and passed for preprocessing. Preprocessing is an important step, as the histopathology images are subjected to different processing stages such as splitting and dyeing [46]. Dehazing algorithm for image enhancement and Gaussian smoothing for noise reduction are used as preprocessing measures in this work. This is followed by identifying threshold values using the MOWOA algorithm. Before the start of the iterations, MOWOA parameters are initialized with maximum iterations, population size, etc. The algorithm begins with arbitrary threshold values. This threshold value is checked to ensure the satisfaction of the defined objective functions. The set of complete Pareto optimal threshold keys forming the Pareto front in the objective space is generated. Then the pareto optimal solution is chosen such that it does not worsen one or the other objective. This procedure is carried out on all the tiles created. Lastly, the algorithm is examined and evaluated by measuring and comparing different metrics like the Dice coefficient, Jaccard index, Accuracy, Precision, F-score, and Specificity against standard processes such as Otsu thresholding with PSO and single-objective WOA.

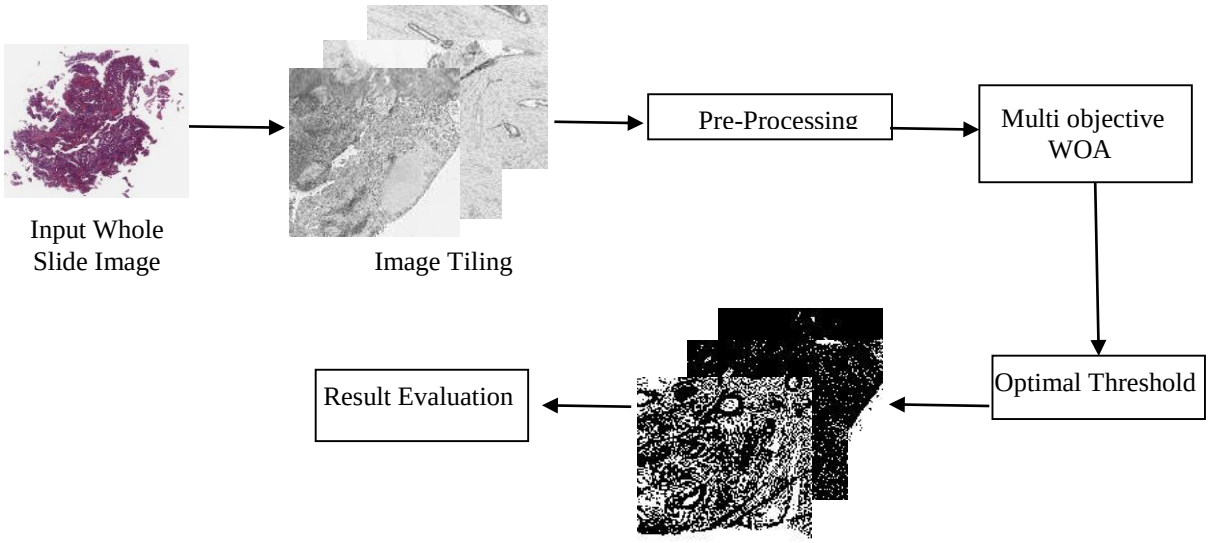

Fig. 1 Workflow of the proposed algorithm

3.1. Otsu Thresholding

Otsu's approach is an image thresholding procedure based on clustering. The process involves classifying image pixels into background and foreground. It works by trying out all possible threshold values and measuring how spread out the pixel intensities are on either side of each threshold.

In other words, it looks at the variation in pixel levels for both the background and the foreground, which is a key part of Otsu's thresholding method.

Consider an image I with N pixels and intensity ranging from 0 to L-1. For this image, let the threshold values be t_0, t_1,…, t_{k-1}. The intensity values range from 0 to t_{0-1}. The pixel probability at the I^{th} intensity level is given as $Pi = \frac{n_i}{N}$, where n_i specifies the overall pixels at the I^{th} level.

The class probabilities are specified by $\omega_0, \omega_1, \ldots, \omega_k$ and the class mean of the sections $R_0, R_1,\ldots R_k$ are $\mu_0, \mu_1, \ldots, \mu_k$, respectively. Each region's mean pixel intensity and probability distribution are represented as:

$$\mu_0 = \sum_{i=0}^{t_0-1} \frac{iP_i}{\omega_0}, \mu_1 = \sum_{i=t0}^{t1-1} \frac{iP_i}{\omega_1}, \ldots\ldots \mu_k = \sum_{i=t0}^{L-1} \frac{iP_i}{\omega_k} \quad (1)$$

$$\omega_0 = \sum_{i=0}^{t_0-1} P_i, \omega_1 = \sum_{i=t0}^{t1-1} P_i, \ldots\ldots\ldots \omega_k = \sum_{i=tk-1}^{L-1} P_i \quad (2)$$

Each class's variance is represented by $\sigma_0^2, \sigma_1^2,\ldots \sigma_k^2$ and is given as:

$$\sigma_0^2 = \omega_0(\mu_0 - \mu_T)^2,\ \sigma_1^2 = \omega_1(\mu_1 - \mu_T)^2, \ldots\ldots, \sigma_k^2 = \omega_k(\mu_k - \mu_T)^2 \quad (3)$$

Where μ_T is the image mean pixel intensity given as:

$$\mu_T = \sum_{i=0}^{L-1} iP_i \quad (4)$$

3.2. Whale Optimization Algorithm

To attain the optimum threshold value for WSI segmentation, this work employs a heuristic Whale Optimization technique, mimicking the actions of whales [11]. Bubbles like spiral circles are created by encircling the prey and then being hunted by the whales, as shown in Figure 2. In this algorithm, the searching agents proceed towards an optimum solution within hypercubes in an n-dimensional search space. The pseudocode of WOA is given below.

First, humpback whales locate their prey and circle them. Then, whales approach the target in a circle, constantly relocating themselves. The mathematical representation is as follows:

$$\vec{D} = \left|\vec{C} \cdot \overrightarrow{X^*}(t) - \vec{X}(t)\right| \quad (5)$$

$$\vec{X}(t+1) = \overrightarrow{X^*}(t) - \vec{A} \cdot \vec{D} \quad (6)$$

where the present iteration is t, coefficient vectors are represented as A and C, and the present location of the search agent is X. With each iteration, a better result is replaced in the vector representing the optimal solution, denoted by X*. The A and C vectors are computed as:

$$\vec{A} = 2\vec{a} \cdot \vec{r} - \vec{a} \quad (7)$$

$$\vec{C} = 2 \cdot \vec{r} \quad (8)$$

Here, 'a' is reduced from 2 to 0 in each repetition, and vector 'r' is an arbitrary value between [0,1]. The updated location of the population is mathematically represented as:

$$\vec{X}(t+1) = \begin{cases} \overrightarrow{X^*}(t) - \vec{A}.\vec{D} & \text{if } p<0.5 \\ \vec{D}.e^{bt}.\cos(2\pi l) + \overrightarrow{X^*}(t) & \text{if } p \geq 0.5 \end{cases} \quad (9)$$

where 'p' is an arbitrary numeral in the range [0, 1], denoting the logarithmic curved profile, l takes values in the range [-1, 1], and 'b', a constant, denotes the spiral's outline

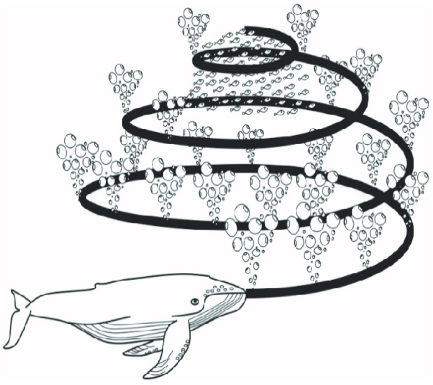

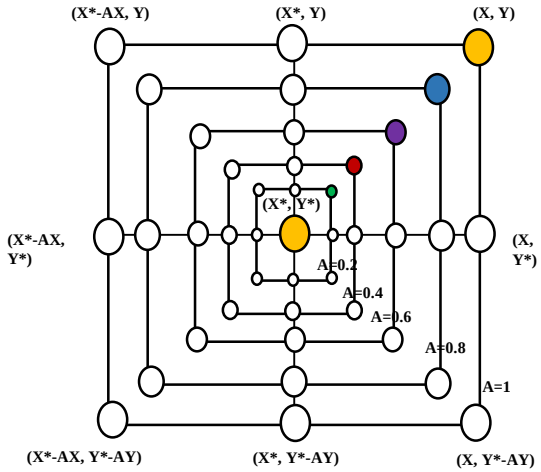

Fig. 2 Hunting behavior in WOA [22]

Pseudocode for the WOA algorithm

```
Whale population initialization
Initialize a, A, C, l, and p
Compute the fitness of all search agents
X* = best search agent
while (t < maximum number of iterations)
   individually update parameters
        if (p < 0.5)
        if (|A| < 1)
           Update current agent position:
           D = |C · X*(t) - X(t)|
           X(t+1) = X*(t) - A · D  (Exploitation phase)
        else if (|A| ≥ 1)
           Select a random search agent (X_rand)
           Update current agent position:
           D = |C · X_rand - X(t)|
           X(t+1) = X_rand - A · D  (Exploration phase)
        end if
      else if (p ≥ 0.5)
        Update current agent position:
        D' = |X*(t) - X(t)|
        X(t+1) = D*e^(bl) cos(2πl) + X*(t)  (Bubble-net
attacking)
      end if
   end for
   Check X going outside the search space and adjust
   Compute each search agent's fitness value
   Update X* with improved result
   t = t + 1
end
return X*
```

3.3. Objective Functions

The three objective functions used in this work comprise maximizing between-class variance, minimizing false positives, and minimizing false negatives. The between-class variance method is a frequently used methodology for image segmentation. This method specifies the degree of diversity between various segments based on pixel values. When a pixel or region is labelled as existing when it does not exist, it is called a false positive. The second objective function aims to minimize these false positives in this work. Another value called false negative occurs when a pixel that belongs to a certain image is labelled as not recognized. This is the third objective function in this work, aiming to minimise false negatives. The mathematical representation of the said objective functions is given below:

$$\text{Objective function 1} = \text{Max}(\sigma^2) \quad (10)$$

where,

$$\sigma^2(t) = P_F(t) * P_B(t) * (\mu_F(t) - \mu_F(t))^2 \quad (11)$$

$$\text{Objective function 2} = \text{Min}\left(\frac{\text{FalsePositive}}{\text{TrueNegative+FalsePositive}}\right) \quad (12)$$

$$\text{Objective function 3} = \text{Min}\left(\frac{\text{FalseNegative}}{\text{TruePositive+FalseNegative}}\right) \quad (13)$$

Here, t is the threshold value, $\sigma^2(t)$ is between class variance, $P_F(t)$ and $P_B(t)$ are probabilities of pixels in foreground and background, respectively, computed using the cumulative distribution function, $\mu_F(t)$ and $\mu_B(t)$ are mean intensities of foreground and background respectively for the given threshold t.

Objective function 1 enhances the distinguishability between pixel classes, leading to improved segmentation performance. Objective function 2 ensures that the model is less likely to incorrectly classify negatives as positives. Objective function 3 ensures the model captures as many true positives as possible, reducing missed detections. Hence, by combining the three objectives, the algorithm balances the trade-offs, such as focusing on accuracy, which leads to poor specificity/sensitivity and vice versa, and thus prevents overfitting to any single metric. Further, this strategy ensures that the optimization problem considers the performance via objective function 1 and the error types through objective functions 2 and 3.

4. Dataset Description

The proposed algorithm's effectiveness in image segmentation was tested by considering five types of whole slide images. The dataset used in this work was drawn from publicly available datasets for study purposes [47, 48]. The size of all the images is 768 x 768 pixels. The details of the images considered in this study are presented in Table 2. A few examples of WSIs with their binary ground masks are shown in Figure 3.

Table 2. Dataset description

Type of cancer	Location	Number of samples	File format
Lung adenocarcinoma	Lungs	25	jpeg
Breast Invasive Carcinoma	Breast	26	jpeg
Corpus Endometrial Carcinoma	Uterus	25	jpeg
Clear Cell Carcinoma	Kidney	26	jpeg
Ductal Adenocarcinoma	Pancreas	16	jpeg

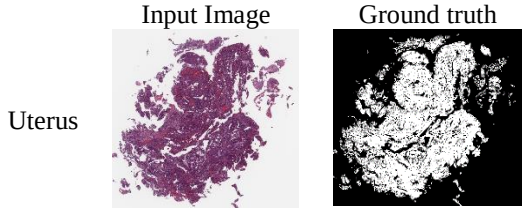

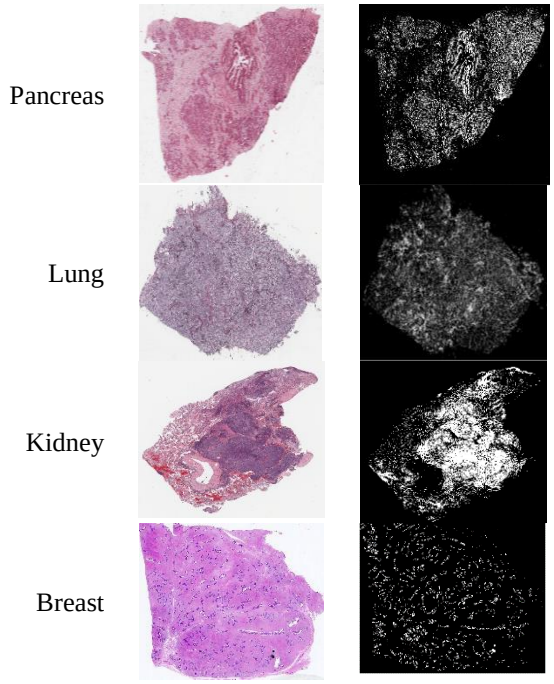

Fig. 3 WSIs with binary ground truth mask

5. Experimental Results

The quality of the pre-processing methodology is evaluated by means of the Structural Similarity Index Measure (SSIM) and the Peak Signal to Noise Ratio (PSNR). While the segmentation algorithm's performance is gauged using metrics such as Dice coefficient, Jaccard coefficient, Precision, Sensitivity, Accuracy, F-measure, and Specificity. The proposed algorithm is executed in MATLAB 2023a.

5.1. Pre-Processing

This phase fixes the slides for segmentation because the slide image undergoes multiple preparation stages and is affected by noise, haze, and low contrast. In this study, RGB photographs are initially converted to grayscale images. Additionally, the histopathological photos are big and challenging to process. As a result, all the photos were tiled using a basic pixel-based tiling approach with dimensions of 128x128. The Dehazing method and Gaussian smoothing were applied to enhance the image and remove noise. The SSIM and PSNR are evaluated to assess the quality of the image after pre-processing [49]. These calculations are performed using:

$$PSNR=20\log_{10}\left(\frac{255}{RMSE}\right)\ dB \tag{14}$$

$$RMSE=\sqrt{\frac{\sum_{i=1}^{r_0}\sum_{j=1}^{c_0}(I_{og}(i,j)-I_{seg}(i,j))^2}{r_0\times c_0}} \tag{15}$$

where I_{og} refers to the actual image, I_{seg} represents the image after segmentation, r_0 and c_0 indicate the image rows and columns numbers. SSIM assesses how similar the actual and segmented images are, and it is calculated using:

$$SSIM(I_{og},I_{seg})=\frac{(2\mu_o\mu_{seg}+c_1)(2\sigma_{o,seg}+c_2)}{(\mu_o^2\mu_{seg}^2+c_1)(\sigma_o^2+\sigma_{seg}^2+c_2)} \tag{16}$$

where μ_0 and μ_{seg} are the mean intensity values, σ_0 and σ_{seg} are the standard deviations of the actual and segmented image. $\sigma_{0,\ seg}$ is the covariance of the initial image and the segmented image, and c_1 and c_2 are constant values. The mean PSNR and SSIM values obtained for each type of WSI are tabulated in Table 3. Higher values are obtained in this proposed work, indicating that the pre-processed image is of better quality than the original image. Once pre-processing is done, histopathology images are segmented using multi-objective thresholding.

Table 3. Quality measurement metrics after preprocessing

Image No.	Image	PSNR	SSIM
1	Uterus	30.46	0.87
2	Pancreas	30.42	0.81
3	Lung	29.92	0.82
4	Kidney	26.39	0 .83
5	Breast	27.32	0.89

5.2. MOWOA Segmentation

This section highlights the results of the MOWOA technique-based segmentation. Table 4 presents the initialization of various parameters for tuning the algorithm. Some of the values are set as default values, and a few are altered in accordance with the best fitness value obtained through trial-and-error iterations.

Table 4. Parameter tuning for the algorithm

Parameters	Values
Population dimension	Number of tiles
Maximum no. of reiterations	100
Position range	[0, 255]
A	[0, 2]
b	1
Fitness functions	3

The proposed method's efficiency is measured by calculating various metrics such as the Dice coefficient, Jaccard coefficient, precision, sensitivity, accuracy, F-measure, and specificity. To measure the competence of the presented system, a comparison is made with other algorithms, including Otsu thresholding combined with PSO, a single-objective WOA that uses between-class variance as its fitness function, WOA optimized to minimize false positives, and WOA designed to reduce false negatives. The dice similarity coefficient is often found to assess how well a segmentation method performs, while the Jaccard Index (JI) assesses the similarity between segmented images and the ground truth images. All the metrics used here are calculated as given below:

$$\text{Dice Index} = \frac{2O \cap S}{O+S} \quad (17)$$

$$\text{Jaccard Index} = \frac{O \cap S}{O \cup S} \quad (18)$$

$$\text{Accuracy} = \frac{TP+TN}{TP+TN+FP+FN} \quad (19)$$

$$\text{Recall/ Sensitivity} = \frac{TP}{TP+FN} \quad (20)$$

$$\text{Specificity} = \frac{TN}{TN+FP} \quad (21)$$

$$\text{Precision} = \frac{TP}{TP+FP} \quad (22)$$

$$\text{F Measure} = 2 \times \frac{\text{Precision} \times \text{Recall}}{\text{Precision}+\text{Recall}} \quad (23)$$

True Positive (TP) refers to the pixels that are properly recognized as part of the area of interest. True Negative (TN) pixels are those that are accurately recognized as unwanted pixels. False Positive (FP) pixels occur when background pixels are mistakenly classified as ROI pixels. Conversely, False Negative (FN) pixels happen when pixels are wrongly labelled as background. Tables 5 - 9 gives the segmentation performance metrics results for all the images considered in this work.

Additionally, Figures 4 (a) - (g) gives a graphical representation of the various metrics for each type of WSI considered in this work. Various performance indices are compared to validate the proposed method. Figure 5 shows the sample segmented image obtained for OPSO and MOWOA. From the images, it is observed that a better-quality segmented image is obtained with the application of MOWOA.

Table 5. Segmentation results for the Uterus image

	OPSO	WOA-BCV	WOA-MFP	WOA-MFN	MOWOA
Mean Dice coefficient	50.25	5, 0.38	50.38	50.38	50.49
Mean JI	49.25	51.62	51.02	51.50	51.62
Mean Precision	50.5	51.62	51.62	51.62	51.62
Mean Recall/sensitivity	70.14	69.00	69.00	69.00	71.57
Mean Accuracy	89.71	91.62	91.62	91.62	92.14
F measure	50.25	50.37	50.37	50.37	50.48
Specificity	68.85	68.00	68.00	68.00	71.57

Table 6. Segmentation results for the Pancreas image

	OPSO	WOA-BCV	WOA-MFP	WOA-MFN	MOWOA
Mean Dice coefficient	48.00	49.63	50.38	51.00	51.50
Mean JI	48.00	50.75	50.75	50.50	51.81
Mean Precision	44.33	50.14	50.42	49.57	51.62
Mean Recall/sensitivity	68.00	72.28	72.14	70.33	69.00
Mean Accuracy	91.57	90.75	90.12	91.14	91.62
F measure	48.33	49.62	51.50	51.00	51.37
Specificity	69.00	68.00	70.10	71.28	68.00

Table 7. Segmentation results for the Lung image

	OPSO	WOA-BCV	WOA-MFP	WOA-MFN	MOWOA
Mean Dice coefficient	48.00	50.38	49.38	50.71	50.75
Mean JI	49.25	49.62	51.25	51.14	51.62
Mean Precision	49.75	51.62	50.75	51.14	51.12
Mean Recall/sensitivity	68.00	69.00	70.85	69.00	72.71
Mean Accuracy	90.14	91.62	90.75	91.14	92.00
F measure	49.62	50.37	49.37	49.81	50.75
Specificity	68.42	68.00	71.60	71.55	72.85

Table 8. Segmentation results for the Kidney image

	OPSO	WOA-BCV	WOA-MFP	WOA-MFN	MOWOA
Mean Dice coefficient	48.00	49.38	51.13	50.38	49.88
Mean JI	48.00	50.25	49.62	50.62	50.75
Mean Precision	44.33	50.75	50.87	51.62	51.12
Mean Recall/sensitivity	68.00	72.85	72.71	69.00	73.28
Mean Accuracy	91.57	90.75	90.62	91.62	92.00
F measure	48.33	49.37	51.12	50.37	49.87
Specificity	69.00	70.60	69.60	68.00	71.60

Table 9. Segmentation results for breast image

	OPSO	WOA-BCV	WOA-MFP	WOA-MFN	MOWOA
Mean Dice coefficient	48.00	50.75	49.50	50.63	51.38
Mean JI	48	49.85	48.88	49.75	50.88
Mean Precision	48.33	50.00	50.88	49.75	50.62
Mean Recall/sensitivity	68.00	72.14	69.00	69.00	71.42
Mean Accuracy	91.57	89.85	90.88	89.75	91.57
F measure	48.33	50.75	49.50	50.62	51.37
Specificity	69.00	68.00	68.00	68.00	71.85

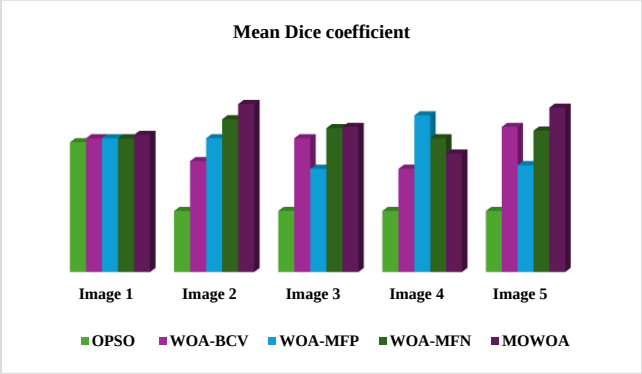

(a)

(b)

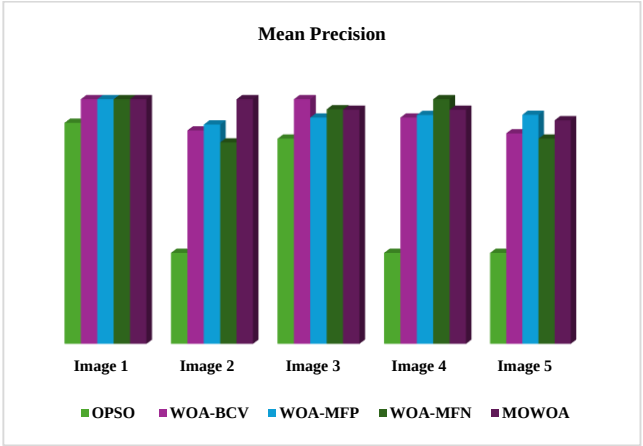

(c)

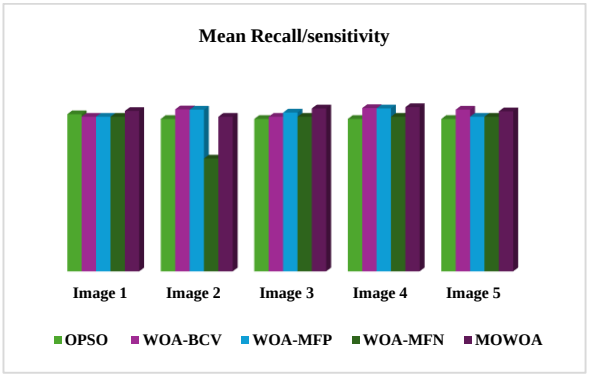

(d)

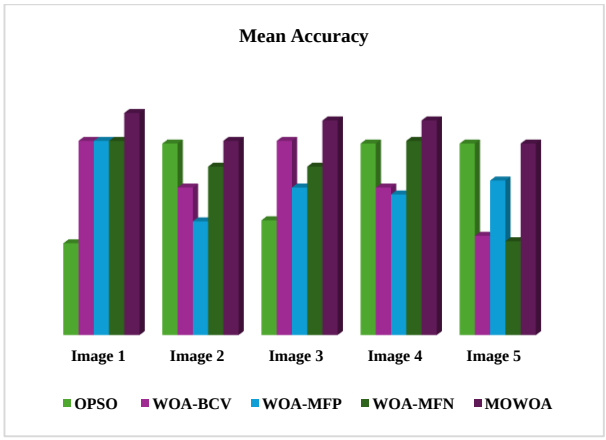

(e)

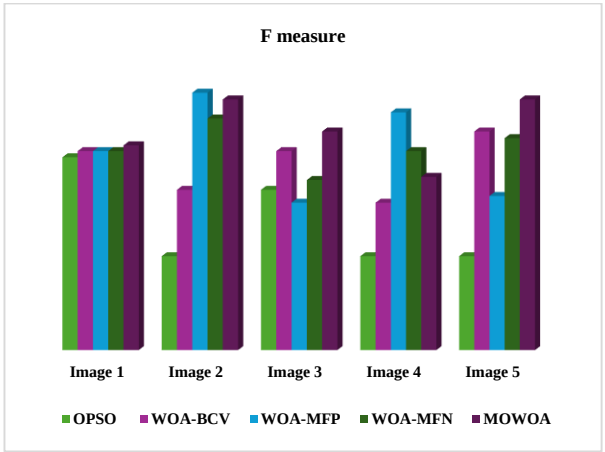

(f)

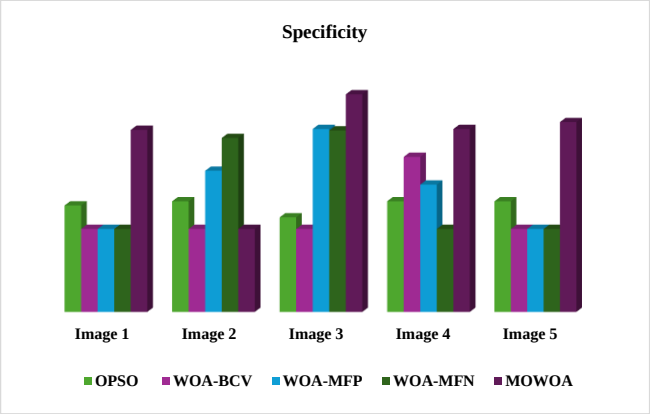

(g)

Fig. 4 (a)-(g) Metrics for the images under consideration

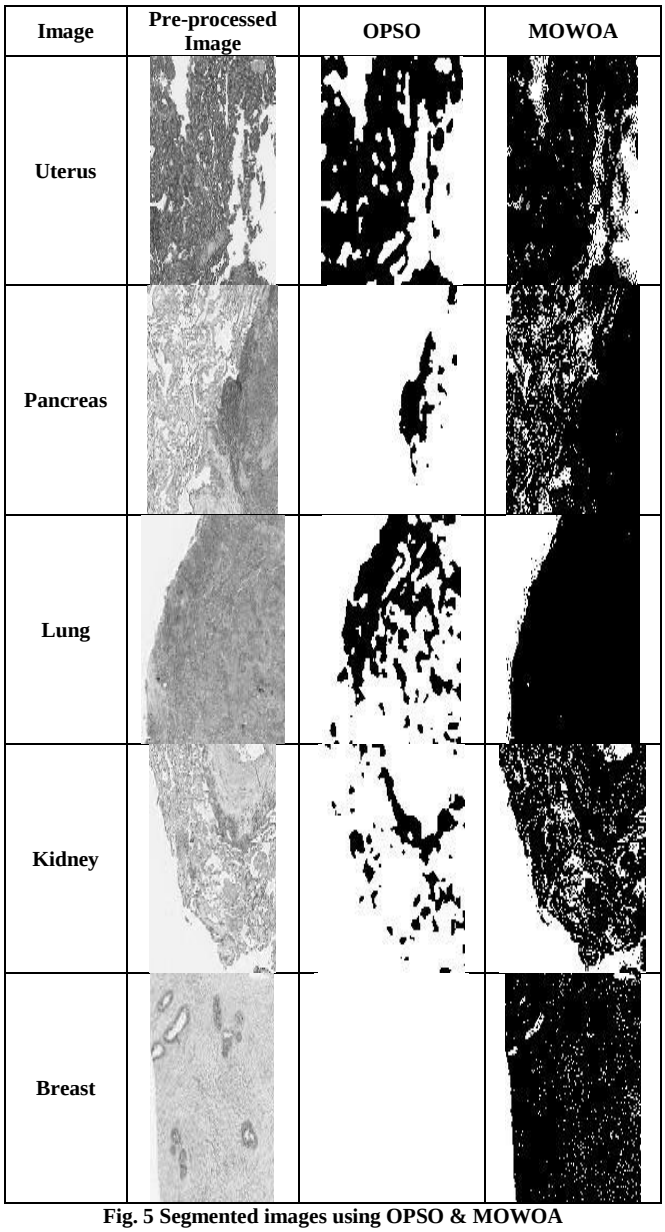

Fig. 5 Segmented images using OPSO & MOWOA

6. Discussion and Inferences

The Multi-Objective Whale Optimization algorithm framework proposed in this work achieved notable and reliable performance across diverse sets of WSIs, as indicated by the experimental results against traditional Otsu-PSO and single objective variants. The fundamental design concepts of MOWOA directly address the shortcomings of existing state-of-the-art methodologies documented in the literature, leading to superior performance. Holistic optimization with three objective functions is one of the reasons for the better performance of the proposed methodology. From the literature review, it is found that the majority of advanced techniques rely on single objective functions. Although these techniques work well for improving a particular metric, they frequently result in uneven performance. A segmentation that maximizes between-class variance, for example, may be very good at distinguishing pixel intensity distributions, but it may also produce many false positives, which would negatively impact accuracy and specificity.

The proposed work directly addresses this shortcoming by formulating the problem as a multi-objective optimization. MOWOA concurrently optimizes between-class variance, minimizes false positives and minimizes false negatives through three objective functions, avoiding single metric overfitting. The findings in Tables 4-8 make it evident that, although single-objective variants occasionally perform better than MOWOA on a particular target metric, for example, WOA-BCV on Recall for pancreatic images, and WOA-MFP on Specificity for kidney images, MOWOA always offers the best overall balance, obtaining high scores on the majority of performance metrics. In medical diagnostics, balanced performance is critical where false positives and negatives have serious clinical repercussions. Additionally, the strong performance of the proposed method across five distinct cancer types from different organs, each with distinct morphological characteristics, demonstrates its robustness. The selection of basic, non-redundant objective functions that are generally relevant to segmentation tasks is what gives the algorithm its generalizability. A well-known benefit of the underlying WOA metaheuristic is that MOWOA successfully traverses the multi-modal search space of thresholding issues without becoming stuck in local optima, as seen by its consistent performance through an accuracy value approximately equal to 92% and a Dice coefficient approximately equal to 51% across all image types. This solves a major problem with other nature-inspired algorithms, such as PSO, which might converge prematurely on sub-optimal solutions for complicated WSI data, as demonstrated by the results.

A high sensitivity value of approximately 72% is noteworthy, since maximizing recall frequently results in a rise in false positives. Also, the proposed algorithm maintains a good Precision value of approximately 52% alongside a high Sensitivity, which is primarily because of the multi-objective

approach. Furthermore, the segmented region and ground truth have superior overlap, as indicated by the Jaccard value of 52% range, which is a strong depiction of unsupervised segmentation. Differences in datasets and evaluation methods make a direct, quantitative comparison difficult for the proposed work, but a qualitative comparison with current research highlights the competitiveness of the outcomes. Several investigations conducted focused on multi-level thresholding, which requires intensive computational power. The proposed work achieves the critical task of segmentation through finding an optimal single threshold via a multi-objective approach.

However, the findings also point to areas that need improvement in the future. The variation in the algorithm's recall for images of the breast and pancreas suggests that the anatomical characteristics of the tissue may have an impact on its capacity to detect all true positives. This implies that using a dynamic, multi-level thresholding strategy catered to a particular cancer type or adding adaptive weights for the objective functions may produce even better outcomes.

The key observations with respect to the methodologies are:

- MOWOA: Frequently attains the highest Mean Dice Coefficient, Jaccard Index, Precision, and Accuracy, consistently performing exceptionally well in most metrics across all workloads. Its ability to strike a balance between identifying real positives and preventing false positives is demonstrated by its strong recall/sensitivity and specificity performance.
- WOA variants: Perform competitively but generally lag behind MOWOA. There is no dominating WOA variety, and strengths differ by measure and image under consideration.
- OPSO: Poorer segmentation performance when compared to WOA-based approaches, as evidenced by consistently lower results across all metrics and tasks.

Table 10 summarizes the overall comparison in terms of various performance metrices and methodologies tried in this work.

Table 10. Comparative summary

Metric	Best Performing Methodology	Remarks
Mean Dice Coefficient	MOWOA	Consistently good value for all the images
Mean Jaccard Index	MOWOA	High values for most of the images, but closely followed by other methods
Mean Precision	MOWOA	Stable performance for all the images
Mean Recall	Varies	WOA-BCV performs well for pancreas and breast images, and MOWOA for other images
Mean Accuracy	MOWOA	Surpasses other methods for all the images
F-measure	MOWOA	Balanced values for most of the images
Specificity	MOWOA / WOA-MFN	WOA-MFN has a higher value for a few images, but generally, MOWOA also performs well

7. Conclusion

Whole slide image segmentation is an important task since efficiency is crucial for the diagnosis of tumors. This work proposed a multi-objective optimization using an inspired Whale Optimization Algorithm for determining the finest threshold value. Various images are tested to validate the proposed methodology. The proposed technique is compared against PSO and WOA with single objective functions. Various metrics proved the competence of the proposed algorithm, achieving an average Dice coefficient of 50.8, Jaccard index of 51.33, Precision value of 51.22, Sensitivity of 71.59, Accuracy of 91.86, F-measure of 50.76, and specificity of 71.17. It is observed that MOWOA performs well on most measures, especially Dice Coefficient, Jaccard Index, and Accuracy.

Recall varies somewhat, with WOA variations occasionally exceeding MOWOA on some images. In comparison to alternative approaches, OPSO underperforms. Future work includes multilevel, multi-objective optimization for thresholding and using hybrid algorithms for WSI segmentation.

References

[1] Anant Madabhushi, and George Lee, “Image Analysis and Machine Learning in Digital Pathology: Challenges and Opportunities,” *Medical Image Analysis*, vol. 33, pp. 170-175, 2016. [CrossRef] [Google Scholar] [Publisher Link]

[2] Péter Bándi et al., “From Detection of Individual Metastases to Classification of Lymph Node Status at the Patient Level: The CAMELYON17 Challenge,” *IEEE Transactions on Medical Imaging*, vol. 38, no. 2, pp. 550-560, 2019. [CrossRef] [Google Scholar] [Publisher Link]

[3] Andrew Janowczyk, and Anant Madabhushi, "Deep Learning for Digital Pathology Image Analysis: A Comprehensive Tutorial with Selected Use Cases," *Journal of Pathology Informatics*, vol. 7, no. 1, 2016. [CrossRef] [Google Scholar] [Publisher Link]

[4] Mahendra Khened et al., "A Generalized Deep Learning Framework for Whole-Slide Image Segmentation and Analysis," *Scientific Reports*, vol. 11, no. 1, pp. 1-14, 2021. [CrossRef] [Google Scholar] [Publisher Link]

[5] Harvey B. Mitchell, *Image Fusion: Theories, Techniques and Applications*, 1st ed., Springer Berlin Heidelberg, pp. 155-161, 2010. [CrossRef] [Google Scholar] [Publisher Link]

[6] Essam H. Houssein et al., "An Efficient Multilevel Image Thresholding Method based on Improved Heap-Based Optimizer," *Scientific Reports*, vol. 13, no. 1, pp. 1-36, 2023. [CrossRef] [Google Scholar] [Publisher Link]

[7] Nobuyuki Otsu, "A Threshold Selection Method from Gray-Level Histograms," *IEEE Transactions on Systems, Man, and Cybernetics*, vol. 9, no. 1, pp. 62-66, 1979. [CrossRef] [Google Scholar] [Publisher Link]

[8] Bong Chin-Wei, and Mandava Rajeswari, "Multiobjective Optimization Approaches in Image Segmentation - The Directions and Challenges," *International Journal of Advances in Soft Computing and its Applications*, vol. 2, no. 1, pp. 1-26, 2010. [Google Scholar] [Publisher Link]

[9] Mohammad Reza Sharifi et al., "A New Optimization Algorithm to Solve Multi-Objective Problems," *Scientific Reports*, vol. 11, no. 1, pp. 1-19, 2021. [CrossRef] [Google Scholar] [Publisher Link]

[10] Niladri Sekhar Datta et al., *A Survey on the Application of Multi-Objective Optimization Methods in Image Segmentation*, Multi-Objective Optimization: Evolutionary to Hybrid Framework, pp. 269-278, 2018. [CrossRef] [Google Scholar] [Publisher Link]

[11] Seyedali Mirjalili, and Andrew Lewis, "The Whale Optimization Algorithm," *Advances in Engineering Software*, vol. 95, pp. 51-67, 2016. [CrossRef] [Google Scholar] [Publisher Link]

[12] S. Nethravathi, and Venkatakirthiga Murali, "A Novel Residential Energy Management System based on Sequential Whale Optimization Algorithm and Fuzzy Logic," *Distributed Generation & Alternative Energy Journal*, vol. 37, no. 3, pp. 557-586, 2022. [CrossRef] [Google Scholar] [Publisher Link]

[13] Nethravathi Shivanaganna, and Venkatakirthiga Murali, "Energy Routing based Optimal Solution for Residential Peak Power Reduction with Photovoltaic and Electric Vehicle Penetration," *Energy Sources, Part A: Recovery, Utilization, and Environmental Effects*, vol. 44, no. 3, pp. 5682-5698, 2022. [CrossRef] [Google Scholar] [Publisher Link]

[14] Metin N. Gurcan et al., "Histopathological Image Analysis: A Review," *IEEE Reviews in Biomedical Engineering*, vol. 2, pp. 147-171, 2009. [CrossRef] [Google Scholar] [Publisher Link]

[15] Sonal Kothari et al., "Pathology Imaging Informatics for Quantitative Analysis of Whole-Slide Images," *Journal of the American Medical Informatics Association*, vol. 20, no. 6, pp. 1099-1108, 2013. [CrossRef] [Google Scholar] [Publisher Link]

[16] Olaf Ronneberger, Philipp Fischer, and Thomas Brox, "U-Net: Convolutional Networks for Biomedical Image Segmentation," *International Conference on Medical Image Computing and Computer-Assisted Intervention*, pp. 234-241, 2015. [CrossRef] [Google Scholar] [Publisher Link]

[17] Ozan Oktay et al., "Attention U-Net: Learning Where to Look for the Pancreas," *arXiv Preprint*, 2018. [CrossRef] [Google Scholar] [Publisher Link]

[18] Hu Cao et al., "Swin-Unet: Unet-Like Pure Transformer for Medical Image Segmentation," *European Conference on Computer Vision*, pp. 205-218, 2023. [CrossRef] [Google Scholar] [Publisher Link]

[19] Michael Kass, Andrew Witkin, and Demetri Terzopoulos, "Snakes: Active Contour Models," *International Journal of Computer Vision*, vol. 1, no. 4, pp. 321-331, 1988. [CrossRef] [Google Scholar] [Publisher Link]

[20] Humayun Irshad et al., "Crowdsourcing Image Annotation for Nucleus Detection and Segmentation in Computational Pathology: Evaluating Experts, Automated Methods, and the Crowd," *Pacific Symposium on Biocomputing Co-Chair*, pp. 294-305, 2015. [CrossRef] [Google Scholar] [Publisher Link]

[21] Jonathan Long, Evan Shelhamer, and Trevor Darrell, "Fully Convolutional Networks for Semantic Segmentation," *2015 IEEE Conference on Computer Vision and Pattern Recognition (CVPR)*, Boston, MA, USA, pp. 3431-3440, 2015. [CrossRef] [Google Scholar] [Publisher Link]

[22] Jieneng Chen et al., "TransUNet: Transformers Make Strong Encoders for Medical Image Segmentation," *arXiv Preprint*, 2021. [CrossRef] [Google Scholar] [Publisher Link]

[23] Shivang Naik et al., "Automated Gland and Nuclei Segmentation for Grading of Prostate and Breast Cancer Histopathology," *2008 5th IEEE International Symposium on Biomedical Imaging: From Nano to Macro*, Paris, France, pp. 284-287, 2008. [CrossRef] [Google Scholar] [Publisher Link]

[24] Yuehong Lu et al., "Comparison of Two Strategies of Reward-Penalty Mechanism for Promoting Net Zero Energy Buildings," *Sustainable Energy Technologies and Assessments*, vol. 47, 2021. [CrossRef] [Google Scholar] [Publisher Link]

[25] Yan Xu et al., "Deep Learning of Feature Representation with Multiple Instance Learning for Medical Image Analysis," *2014 IEEE International Conference on Acoustics, Speech and Signal Processing (ICASSP)*, Florence, Italy, pp. 1626-1630, 2014. [CrossRef] [Google Scholar] [Publisher Link]

[26] Salar Razavi et al., "MiNuGAN: Dual Segmentation of Mitoses and Nuclei using Conditional GANs on Multi-Center Breast H&E Images," *Journal of Pathology Informatics*, vol. 13, pp. 1-9, 2022. [CrossRef] [Google Scholar] [Publisher Link]

[27] Juan Wang *et al.*, "Nuclei Instance Segmentation using a Transformer-Based Graph Convolutional Network and Contextual Information Augmentation," *Computers in Biology and Medicine*, vol. 167, pp. 1-16, 2023. [CrossRef] [Google Scholar] [Publisher Link]

[28] Gabriele Campanella et al., "Clinical-Grade Computational Pathology using Weakly Supervised Deep Learning on Whole Slide Images," *Nature Medicine*, vol. 25, no. 8, pp. 1301-1309, 2019. [CrossRef] [Google Scholar] [Publisher Link]

[29] Qiang Li et al., "Rapid Whole Slide Imaging via Dual-Shot Deep Autofocusing," *IEEE Transactions on Computational Imaging*, vol. 7, pp. 124-136, 2021. [CrossRef] [Google Scholar] [Publisher Link]

[30] Essam H. Houssein, Marwa M. Emam, and Abdelmgeid A. Ali, "Improved Manta Ray Foraging Optimization for Multi-Level Thresholding using COVID-19 CT Images," *Neural Computing and Applications*, vol. 33, no. 24, pp. 16899-16919, 2021. [CrossRef] [Google Scholar] [Publisher Link]

[31] Mohamed Abdel-Basset, Victor Chang, and Reda Mohamed, "A Novel Equilibrium Optimization Algorithm for Multi-Thresholding Image Segmentation Problems," *Neural Computing and Applications*, vol. 33, no. 17. pp. 10685-10718, 2021. [CrossRef] [Google Scholar] [Publisher Link]

[32] Qian Zhang et al., "Gaussian Barebone Salp Swarm Algorithm with Stochastic Fractal Search for Medical Image Segmentation: A COVID-19 Case Study," *Computers in Biology and Medicine*, vol. 139, pp. 1-31, 2021. [CrossRef] [Google Scholar] [Publisher Link]

[33] S. Pare et al., "A New Technique for Multilevel Color Image Thresholding based on Modified Fuzzy Entropy and Lévy Flight Firefly Algorithm," *Computers & Electrical Engineering*, vol. 70, pp. 476-495, 2018. [CrossRef] [Google Scholar] [Publisher Link]

[34] Essam H. Houssein et al., "A Novel Black Widow Optimization algorithm for Multilevel Thresholding Image Segmentation," *Expert Systems with Applications*, vol. 167, 2021. [CrossRef] [Google Scholar] [Publisher Link]

[35] Falguni Chakraborty, Provas Kumar Roy, and Debashis Nandi, "Oppositional Elephant Herding Optimization with Dynamic Cauchy Mutation for Multilevel Image Thresholding," *Evolutionary Intelligence*, vol. 12, no. 3, pp. 445-467, 2019. [CrossRef] [Google Scholar] [Publisher Link]

[36] Yi Liu et al., "Modified Particle Swarm Optimization-Based Multilevel Thresholding for Image Segmentation," *Soft Computing*, vol. 19, no. 5, pp. 1311-1327, 2015. [CrossRef] [Google Scholar] [Publisher Link]

[37] Sunil L. Bangare et al., "Reviewing Otsu's Method for Image Thresholding," *International Journal of Applied Engineering Research*, vol. 10, no. 9, pp. 21777-21783, 2015. [CrossRef] [Google Scholar] [Publisher Link]

[38] Senthilkumaran N., and Vaithegi S., "Image Segmentation By using Thresholding Techniques For Medical Images," *Computer Science & Engineering: An International Journal (CSEIJ)*, vol. 6, no. 1, pp. 1-13, 2016. [CrossRef] [Google Scholar] [Publisher Link]

[39] Liang-Kai Huang, and Mao-Jiun J. Wang, "Image Thresholding by Minimizing the Measures of Fuzziness," *Pattern Recognition*, vol. 28, no. 1, pp. 41-51, 1995. [CrossRef] [Google Scholar] [Publisher Link]

[40] Yanqiao Zhao et al., "A Fast 2-D Otsu Lung Tissue Image Segmentation Algorithm based on Improved PSO," *Microprocessors and Microsystems*, vol. 80, pp. 1-8, 2021. [CrossRef] [Google Scholar] [Publisher Link]

[41] Shamsuddeen Adamu et al., "Unleashing the Power of Manta Rays Foraging Optimizer: A Novel Approach for Hyper-Parameter Optimization in Skin Cancer Classification," *Biomedical Signal Processing and Control*, vol. 99, 2025. [CrossRef] [Google Scholar] [Publisher Link]

[42] Maryam Mohammdian-khoshnoud et al., "Optimization of Fuzzy C-Means (FCM) Clustering in Cytology Image Segmentation using the Gray Wolf Algorithm," *BMC Molecular and Cell Biology*, vol. 23, no. 1, pp. 1-9, 2022. [CrossRef] [Google Scholar] [Publisher Link]

[43] Thavavel Vaiyapuri, and Haya Alaskar, "Whale Optimization for Wavelet-Based Unsupervised Medical Image Segmentation: Application to CT and MR Images," *International Journal of Computational Intelligence Systems*, vol. 13, no. 1, pp. 941-953, 2020. [CrossRef] [Google Scholar] [Publisher Link]

[44] Anusree Kanadath, J. Angel Arul Jothi, and Siddhaling Urolagin, "Multilevel Colonoscopy Histopathology Image Segmentation using Particle Swarm Optimization Techniques," *SN Computer Science*, vol. 4, no. 5, 2023. [CrossRef] [Google Scholar] [Publisher Link]

[45] Krishna Gopal Dhal et al., "Breast Histopathology Image Clustering using Cuckoo Search Algorithm," *Proceedings of the 5th Student Computer Science Research Conference*, pp. 47-54, 2018. [CrossRef] [Google Scholar] [Publisher Link]

[46] Massimo Salvi et al., "The Impact of Pre- and Post-Image Processing Techniques on Deep Learning Frameworks: A Comprehensive Review for Digital Pathology Image Analysis," *Computers in Biology and Medicine*, vol. 128, pp. 1-24, 2021. [CrossRef] [Google Scholar] [Publisher Link]

[47] Larxel, Lung and Colon Cancer Histopathological Images, Kaggle, 2019. [Online]. Available: https://www.kaggle.com/datasets/andrewmvd/lung-and-colon-cancer-histopathological-images/

[48] CDSA, Digital Slide Archive (DSA), 2025. [Online]. Available: https://cancer.digitalslidearchive.org/#!/CDSA/acc/TCGA-OR-A5J1

[49] Zhou Wang et al., "Image Quality Assessment: From Error Visibility to Structural Similarity," *IEEE Transactions on Image Processing*, vol. 13, no. 4, pp. 600-612, 2004. [CrossRef] [Google Scholar] [Publisher Link]